TUMOR PROGRESSION AND PHARMACOLOGICAL INTERVENTION: MODELING IMMUNOTHERAPEUTIC AND CHEMOTHERAPY STRATEGIES IN NEUROBLASTOMA

Kate Brockman[2], Brian Colburn[1], Joseph Garza[3], Yidong Liao[1], and BV Shankara Narayana Rao[1]

[1]*Department of Mathematics and Statistics, Texas A&M University - Corpus Christi*
[2]*Department of Engineering, Texas A&M University - Corpus Christi*
[3]*Department of Life Sciences, Texas A&M University - Corpus Christ*

Abstract. Neuroblastoma is one of the most common solid tumors found in children and is one of the leading cause of childhood cancer. Even with advancements in treatment, there is still a need for optimal therapies and more accurate mathematical models that have the potential to guide clinical decision-making for neuroblastoma patients. Among the available treatments, immunotherapy and chemotherapy, particularly the use of Interleukin-2 (IL-2) and Cyclophosphamide, have shown encouraging results by enhancing the immune-response and targeting cancerous cells. In this study, we developed a nonlinear system of coupled first-order differential equations to simulate the interactions between tumor cells, natural killer (NK) cells, and cytotoxic T lymphocytes (CTLs). The model accounted for the effects of IL-2 and Cyclophosphamide on these immune cell populations. By examining tumor dynamics across different patient risk groups, the model provides a framework for optimizing therapeutic strategies and improving clinical outcomes in neuroblastoma treatment.

1. Introduction. Cancer is characterized as a disease associated by uncontrolled proliferation of abnormal cells. These cells invade and disrupt surrounding healthy tissue and has been proved to be driven by a combination of genetic predispositions, environmental exposures, and lifestyle related factors [15]. Neuroblastoma, in paticular is the most common tumor growth in children under the age of four year old, and it holds a significant place in pediatric oncology due to its high prevalence. The cancer typically comes about in infants within their first year of life and may present as either localized or widespread metastatic disease [16]. Neuroblastoma patients have hisorically been classified into various risk categories: low, intermediate, and high, based on the International Neuroblastoma Risk Group (INRG) staging system (Table 1), which takes into account factors such as age, tumor stage, histology, and genetic components. For low risk patients, who have an estimated survival rate above 98%, observation or surgical resection is normally sufficient for tumor redaction. Intermediate-risk patients with survival rates exceeding 90%, often receive chemotherapy in combination with surgery. In contrast, high-risk patients undergo a multi-approach regimen that includes multiple cycles of chemotherapy, surgical resection, radiation and immunotherapy [2]. This standardized risk-differentiated patient classification system facilitates better survival outcomes by providing an objective framework to optimize treatment strategies in neuroblastoma, whilst minimizing long-term adverse effects of the treatment. Given the increasing use of immunotherapies in treatment regimens, a deeper understanding of the immune system's role in tumor control has become essential [1].

Biologically speaking, the immune response and system to cancer involves a two-part immune system response: the innate and adaptive immune systems. Each contribute uniquely to tumor recognition and elimination. In this study, NK cells were modeled in association with the innate immune system, representing rapid and non-specific responses to cancerous cells. CTLs, by contrast, are cells of the adaptive immune system and mount antigen-specific responses following activation and clonal expansion [8]. This differentiation is central to the development of a immunotherapeutic modeling framework, as it reflects differences in cell activation timing and therapeutic targeting. By incorporating both NK cells and CTLs into the developed objective pharmacology model, we capture the complementary roles of innate and adaptive immunity in shaping tumor–immune dynamics under various treatment conditions. These differences form the foundation for simulating immune responses across various patient risk categories and treatment regimens.

Historically, mathematical modeling has played an important role in cancer research, bridging the gap between theoretical biology and clinical applications [3-5,7,10,13,17]. As the biological understanding of cancer has increased, mathematical and computational models have become essential tools for integrating diverse data types and biological processes into mechanistic frameworks capable of simulating the treatment outcomes of cancer patients [13]. In the context of neuroblastoma, models such as the one presented offer valuable insights into tumor progression, therapeutic response, and theoretical disease evolution. They support a wide range of applications, including the optimization of chemotherapy scheduling, immunotherapy planning, and personalized treatment strategies. Furthermore, these models enable the formulation of testable hypotheses and the incorporation of experimental and clinical data into predictive simulations [13]. However, despite their promise, oncological modeling is challenged by the inherent complexity of biological systems and the rigorous demands of model validation, verification, and clinial integration.

2. Methods. Building on a previously established framework by Song [17], this study modeled the cellular interactions between tumor cells, NK cells, and CTLs, with modifications to incorporate the therapeutic effects

of two drugs used for the treatment of neuroblastoma. The mathematical framework was developed as a set of coupled, first-order ordinary differential equations to represent immune–tumor population dynamics under various pharmacological states.

2.1. Therapeutic agent selection. Two therapeutic agents were selected for the modeling of neuroblastoma treatment: Cyclophosphamide and IL-2. These drugs were chosen for their complementary mechanisms. Cyclophosphamide acts through direct tumor cell cytotoxicity, whilst IL-2 enhances immune system activation and function. By incorporating both of these agents into our model, we aimed to quantify how chemotherapy induced tumor cell death and immune mediated tumor suppression operate independently and synergistically. This approach allowed us to explore the balance between direct cytotoxic effects and immune system activation across different stages of patient diseases.

Cyclophosphamide, a chemotherapy drug, directly targets tumor cells by slowing the rate at which they proliferate and inducing apoptosis. It alkylates DNA, leading to the formation of crosslinks that interfere with replication and trigger cell death, in particular with rapidly dividing cells. Beyond its direct cytotoxicity, Cyclophosphamide controls the tumor microenvironment by suppressing immune responses [6]. Despite its immunosuppressive effects, its potent ability to reduce tumor burden makes it a cornerstone in neuroblastoma treatment in modern medicine.

IL-2, an immune-modulating cytokine, plays a critical role in activating NK cells, which are essential for the innate immune response against tumor cell development. IL-2 binds to receptors in NK cells, promoting proliferation, activation, and cytotoxicity. Activated NK cells then directly eliminate tumor cells by releasing perforin and granzymes, inducing apoptosis [14]. IL-2 enhances the expression of activating receptors in NK cells, improving their ability to recognize and target tumor cells, and esepcially early on in the immune defense. In neuroblastoma treatment, this immune activation supports a shift toward a a tumor-targeting immune environment [14].

2.2. Objective pharmacology model. The objective pharmacological model developed in this study shows the immune–tumor dynamics of neuroblastoma progression and evaluates it's therapeutic effects on immunotherapy and chemotherapy treatments. The model (Equation 2.1) integrates key biological processes including tumor growth, immune activation, and drug-induced modulation of immune responses. By simulating tumor progression across low, intermediate, and high-risk patient profiles, the framework offered insights into optimizing treatment strategies and informing personalized therapeutic interventions.

$$\begin{cases} N'(t) = a_1 N(t)(1 - bN(t)) - a_2 N(t) - \alpha_1 N(t)T(t) + k_i I(t) \\ L'(t) = r_1 N(t)T(t) - \mu L(t) - \beta_1 L(t)T(t) \\ T'(t) = cT(t)(1 - dT(t)) - \alpha_2 N(t)T(t) - \beta_2 L(t)T(t) - k_c C(t) \\ I'(t) = -\dfrac{\log(2)}{h_i} 2^{-\frac{t}{h_i}} I(0) \\ C'(t) = -\dfrac{\log(2)}{h_c} 2^{-\frac{t}{h_c}} C(0) \end{cases} \tag{2.1}$$

Let $N(t)$, $L(t)$, and $T(t)$ represent the populations of NK cells, CTLs, and tumor cells, while $I(t)$ and $C(t)$ denote the concentrations of IL-2 and Cyclophosphamide.

2.2.1. Scaling and nondimensionalization. To reduce model complexity and highlight biological mechanisms, the system was nondimensionalization (Equation 2.2) using scaling factors. This approach reformulates the equations in terms of dimensionless variables and parameters, allowing for a more straightforward interpretation and comparison across treatment groups.

$$\begin{cases} N'(t) = p_1 N(t)(1 - qN(t)) - p_2 N(t) - N(t)T(t) + k_i I(t) \\ L'(t) = N(t)T(t) + rD(t) - L(t) - sL(t)T(t) \\ T'(t) = uT(t)(1 - vT(t)) - N(t)T(t) - \delta L(t)T(t) - k_c C(t) \\ I'(t) = -\dfrac{\log(2)}{h_i} 2^{-\frac{t}{h_i}} I(0) \\ C'(t) = -\dfrac{\log(2)}{h_c} 2^{-\frac{t}{h_c}} C(0) \end{cases} \tag{2.2}$$

The simplification brings about parameters $p_1 = \frac{a_1}{\mu}$ and $p_2 = \frac{a_2}{\mu}$, which normalize the NK cell proliferation and natural death rates relative to the CTL death rate μ. The parameter $q = \frac{b}{\mu\alpha_2}$ represents the NK cell carrying

capacity scaled by the NK-induced tumor cell death rate. The term $r = \frac{T(0)}{\alpha_1 \alpha_2} \cdot \frac{r_1}{\mu}$ accounts for CTL activation resulting from tumor cell byproducts generated by NK induced cytotoxicity, scaled by the initial tumor burden. The parameter $s = \frac{\beta_1}{\alpha_1}$ expresses the relative rates at which CTLs and NK cells are lost through interactions with tumor cells. The tumor growth rate is scaled as $u = \frac{c}{\mu}$, and the term $v = \frac{du}{\alpha_1}$ captures the effects of tumor carrying capacity modulated by NK activity. Finally, $\delta = \frac{\beta_2 r_1}{\alpha_1 \alpha_2}$ characterizes the CTL-induced tumor cell death rate relative to that of NK cells. Together, these nondimensionalized parameters (Table X) highlight the dominant mechanisms governing tumor–immune dynamics and enable a more generalized analysis across treatments and patient disease profiles.

2.2.2. Parameter selection. The initial conditions and parameters used in the model were informed by the interactions among tumor progression, drug concentration, and patient population, and were tailored to disease stage, with modifications adapted from the literature [5]. This framework optimized treatment planning by simulating clinical for specific patient groups. Our approach to modeling the immunotherapeutic dynamics of neuroblastoma is grounded in the International Neuroblastoma Risk Group (INRG) staging system [9], which significantly enhanced our ability to compare patient populations in the context of therapeutic interventions.

Table 1: Neuroblastoma disease stages defined by the International Neuroblastoma Risk Group.

Disease Stage	Description
Low Risk	Patients with L1 (localized tumors in one area) or MS (asymptomatic with favorable biology and metastases limited to skin, liver, or bone marrow) are considered low risk. These patients typically require observation, with surgery or chemotherapy only if symptoms arise.
Intermediate Risk	L2 (regional tumors with IDRFs) and MS with unfavorable biology (e.g., diploidy) are classified as intermediate risk. These tumors may need chemotherapy, with surgery recommended if possible.
High Risk	M (distant metastases), MS with MYCN amplification, or L2 in patients over 18 months with unfavorable features are high risk. These patients require aggressive treatment including chemotherapy, surgery, and stem cell therapy.

In this study, we employed the INRG staging system to stratify patient populations into low, intermediate, and high-risk groups based on tumor stage (Table 1). This classification system supported the comparative analyses across trials and informed our initial conditions for the mathematical model. By aligning with an internationally accepted risk framework, we enhanced the clinical relevance and reproducibility of our simulations.

For each risk group, we estimated the relative initial abundances of tumor cells, CTLs, and NK cells, whilst paying particular attention to capturing the relative population sizes (Table 2). These differentiated immune profiles enabled a more accurate simulations of treatment outcomes under varying immunological baselines and allowed us to explore how the immune composition influences therapeutic responses.

Table 2: Initial cell populations by neuroblastoma risk group.

Cell Population	Low Risk	Intermediate Risk	High Risk
$N(0)$	–	–	–
$L(0)$	–	–	–
$T(0)$	–	–	–

The low-risk population was characterized by a low tumor cell count and an highly active immune response, where NK cells, part of the innate immune system, offerd immediate defense to tumor cells. While CTLs, which belong to the adaptive immune response, provided a targeted and more long-term defense, their abundance is lower compared to NK cells. In the intermediate-risk population, the tumor cell count is higher, showing a more significant role for CTLs in the immune response. Though NK cells still serve as the first line of defense, the increased tumor burden necessitates a coordinated immune response, with CTLs becoming increasingly critical for targeting and eliminating the growing tumor cells. In the high-risk population, the tumor cell count is elevated, and the immune system faces greater challenges. While NK cells provided an early line of defense and gradually declined over time, CTLs proved to be essential for long-term tumor control. CTLs ability to recognize specific

antigens and undergo clonal expansion enabled a more sustained immune response against the rapidly proliferating tumor cells.

Table 3: Pharmacology model parameters.

Parameter	Description	Units	Value
a_1	NK cell growth rate	cell $\cdot$ day^{-1}	0.111
a_2	NK cell death rate due to natural death	day^{-1}	0.0412
b	Carrying capacity coefficient for NK cell population	cell^{-1}	1.02e-09
c	Natural tumor cell growth rate	day^{-1}	0.514
d	Carrying capacity coefficient for tumor cell population	cell^{-1}	1.02e-09
α_1	Rate of NK cell death due to tumor interaction	cell^{-1} $\cdot$ day^{-1}	1e-07
α_2	Rate of NK-induced tumor death	cell^{-1} $\cdot$ day^{-1}	3.23e-07
β_1	Rate of CTL-cell death due to tumor interaction	cell^{-1} $\cdot$ day^{-1}	3.422e-10
β_2	Rate of CTL-induced tumor death	cell^{-1} $\cdot$ day^{-1}	0.01245
μ	CTL cell death rate due to natural death	day^{-1}	0.02
r_1	Rate of NK-lysed tumor cell debris activation of CTLs	cell^{-1} $\cdot$ day^{-1}	2.908e-11
k_c	Rate constant of Cyclophosphamide-mediated tumor death	mg^{-1} $\cdot$ day^{-1} $\cdot$ cell	0.9
k_i	Rate constant of IL-2-mediated stimulation	mg^{-1} $\cdot$ day^{-1} $\cdot$ cell	5e+04
h_i	Half-life of IL-2	day	–
h_c	Half-life of Cyclophosphamide	day	–
I_0	Dose of IL-2	mg	–
C_0	Dose of Cyclophosphamide	mg	–

Model parameters (Table 3) were selected to reflect biological processes driving neuroblastoma progression, immune system interactions, and the therapeutic effects of IL-2 and Cyclophosphamide. NK cell populations were regulated by intrinsic growth (a_1), death (a_2), and a carrying capacity constraint (b), while tumor-induced cytotoxicity was governed by the interaction rate (α_1). CTL dynamics were shaped by activation through NK-lysed tumor byproducts (r_1), natural cell death (μ), and tumor-induced depletion (β_1). Tumor proliferation was defined by the growth rate (c) and the carrying capacity (d), with immune-mediated reduction captured by NK and CTL-mediated lysis (α_2, β_2).

Drug-related parameters chosen included the rate of IL-2 stimulation of NK cells (k_i) and the rate of Cyclophosphamide induced tumor reduction (k_c), both of which play important roles in modulating immune response and tumor grwoth in neuroblastoma. Their concentrations were modeled using first-order exponential decay based on pharmacokinetic half-lives (h_i, h_c), capturing the transient nature of these agents in systemic circulation. Initial dosages of IL-2 (I_0) and Cyclophosphamide (C_0) define the dosing schedule for treatment simulations (Table 3).

2.2.3. Pharmacological schedules. Dosing schedules for Cyclophosphamide and Interleukin-2 (IL-2) were differentiated by treatment intensity (low-dose and high-dose) and divided into initial and recurring administrations. For Cyclophosphamide, low-dose treatment involved an initial dose of 2.5 mg/kg followed by recurring doses of 2 mg/kg every 24 hours. High-dose treatment began with an initial dose of 30 mg/kg, with recurring doses of 25 mg/kg administered at 24-hour intervals [6]. IL-2 was administered on a fixed 24-hour cycle. Low-dose schedules involved an initial and recurring dose of 3×10^6 units, while high-dose schedules used 6×10^6 units per dose on the same interval [12].

Table 4: Dosing schedules for Cyclophosphamide and Interleukin-2.

Drug	Schedule	Initial Dose	Recurring Dose
Cyclophosphamide	Low-dose	2.5 mg/kg	2 mg/kg
Cyclophosphamide	High-dose	30 mg/kg	25 mg/kg
IL-2	Low-dose	3×10^6 units	3×10^6 units
IL-2	High-dose	6×10^6 units	6×10^6 units

2.3. Caputo fractional order derivative framework. To enhance the biological nature of our neuroblastoma model, we incorporated a Caputo fractional-order derivative to capture tumor dynamics. This framework

applied to three of the differential equations in our system being that of CTL, NK, and Tumor cells, excluding the drug/treatment variables. The Caputo Operator showed to improve the accuracy of tumor growth modeling by accounting for historical system behavior, as demonstrated in recent studies [10]. By applying this approach, we refined the characterization of tumor-immune interactions and treatment efficacy across neuroblastoma patient groups.

Tumor cells, CTLs, and NK cells are denoted by T,L, and N respectively. All other parameters are defined in Table 3.

Definition 1 Consider the following function $\varphi(t)$, when $t > 0$, and the Riemann-Liouville Integral (RLI) operator of a function $\varphi(t)$ is defined as follows:

$$I^{\alpha}\varphi(t) = \int_0^t \frac{(t-\tau)^{\alpha-1}}{\Gamma(\alpha)}\varphi(\tau)\,d\tau \tag{2.3}$$

$\alpha > 0$ is the order derivative and x(t), y(t), and z(t) represent the respective population of NK, CTLs, and Tumor cells. The fractional derivative operator is denoted D_0^{α} and $\alpha > 0$ defines the fractional order allowing to model memory and hereditary effects better than the classical integer order derivatives when $\alpha > 0$ lies between the integer values and the gamma function are the generalization of the factorial function to continuous values, and $(t-\tau)^{\alpha-1}$ is the kernel function that is being integrated and gives the fractional derivative its memory property, where τ is a past time point on the interval [0,t].

The fractional-order derivative of function $\varphi(t)$ in [equation 1] is defined by the following:

$$D^{a}\varphi(t) = I^{n-a}D^{(n)}\varphi(t) \tag{2.4}$$

where D= d/dt

Definition 2 Consider the function $\varphi(t)$ when $t > 0$, the Caputo fractional derivative of order α when $\alpha > 0$ is given by the following:

$$D^{\alpha}\varphi(t) = \frac{1}{\Gamma(n-\alpha)}\int_0^t (t-\tau)^{n-\alpha-1}\varphi^{(n)}(\tau)\,d\tau \tag{2.5}$$

where n is the nth derivative, α belongs to (n-1,n) and $D^{\alpha}\varphi(t)$ is the Caputo fractional operator of the function $\varphi(t)$.

Theorem 1 Consider a system of fractional order equations in the form:

$$D_0^{a}\varphi(t) = \varphi(t, Y(t)), Y(t_0) = Y_0 \tag{2.6}$$

The following statements will be true when J(Y*) is the Jacobian Matrix:

- The equilibrium point is asymptotically stable only if all eigenvalues of the Jacobian Matrix satisfy $\arg\lambda_i > a\pi/2$ from 2.21 and 2.22
- The equilibrium point is unstable only if all eigenvalues of the Jacobian Matrix such that $\arg\lambda_i < a\pi/2$ from 2.21 and 2.22

Here we generalize an integer-order tumor interaction model, given by the following equations (2.7)–(2.9) is a set that is a continuous nonlinear ordinary differential equation:

$$N'(t) = \alpha_1 N(t)(1 - bN(t)) - \alpha_2 N(t) - \alpha_1 N(t)T(t) \tag{2.7}$$

$$L'(t) = r_1 N(t)T(t) + r_2 D(t) - \mu L(t) - \beta_1 L(t)T(t) \tag{2.8}$$

$$T'(t) = cT(t)(1 - dT(t)) - \alpha_2 N(t)T(t) - \beta_2 L(t)T(t) \tag{2.9}$$

where N, L, and T represent the populations of the natural killer cells, CTL cells, and tumor cells respectively. Furthermore α_1, α_2, b, r_1, r_2, μ, β_1, β_2, and c are all parameters from Table3.

After non-dimensionalizing equations (2.7)–(2.9), we get the following equations:

$$N'(t) = p_1 N(t)(1 - qN(t)) - p_2 N(t) - N(t)T(t) \tag{2.10}$$

$$L'(t) = N(t)T(t) + rD(t) - L(t) - sL(t)T(t) \tag{2.11}$$

$$T'(t) = uT(t)(1 - vT(t)) - N(t)T(t) - (\delta)L(t)T(t) \tag{2.12}$$

where p_1, p_2, q, r, s, u, v, and δ are the nondimensional parameters. Now the proposed dimensionless model is put into Caputo fractional order derivative form with the following equations:

$$D_0^\alpha, x(t) = p_1 x(t)(1 - qx(t)) - p_2 x(t)z(t) \tag{2.13}$$

$$D_0^\alpha, y(t) = x(t)z(t) + rd(t) - y(t) - sy(t)z(t) \tag{2.14}$$

$$D_0^\alpha, z(t) = uz(t)(1 - vz(t)) - x(t)z(t) - \delta y(t)z(t) \tag{2.15}$$

when $\alpha > 0$ is the order derivative and x(t), y(t), and z(t) represents the respective cell population of the natural killer (NK) cells, the cytotoxic t lymphocytes (CTL) and the tumor (T).

2.4. Existence of Unique Solutions. In this section, the existence of a unique solution of the fractional order tumor model will be proved with the help of a lemma and definitions.

Lemma 1. Consider the system of equations defined by Caputo fractional-order derivatives:

$$D^a x(t) = p_1 x(1 - qx) - p_2 xz \tag{2.16}$$

$$D^a y(t) = xz + rd - y - syz \tag{2.17}$$

$$D^a z(t) = uz(1 - vz) - xz - \delta yz \tag{2.18}$$

where $0 < a \leq 1$. Then the system admits a unique solution under appropriate conditions, ensuring that disturbances in initial conditions do not lead to non-deterministic behaviors. This reinforces the stability of the fractional-order system.

The initial conditions of the fractional order derivatives can be written as $x(t_0) = x_0, y(t_0) = t_0$, and $z(t_0) = z_0$. Equations (2.13)–(2.15) can be written in the form:

$$D^a Y(t) = R_1 Y(t) + x(t)R_2 Y(t), Y(t_0) = Y_0 \tag{2.19}$$

where Y_0 are initial conditions of the function Y(t) which is the column vector of the equations x(t), y(t), and z(t) are the respective population equations of natural killer cells, cytotoxic t-lymphocyte cells, and tumor cells

$$Y(t) = \begin{bmatrix} x(t) \\ y(t) \\ z(t) \end{bmatrix} \tag{2.20}$$

$$R_1 = \begin{bmatrix} 0 & 0 & 0 \\ 0 & -1 & 0 \\ u & 0 & v \end{bmatrix} \tag{2.21}$$

$$R_2 = \begin{bmatrix} p_1(1-q) & 0 & -p_2 \\ 1 & 0 & 0 \\ -1 & -\delta & -1 \end{bmatrix} \tag{2.22}$$

The following definitions are required for the existence and uniqueness of solutions for equation 2.19 .

Definition 3 Consider C[0,θ] to belong to a continuous vector Y(t) with the components of functions of x(t), y(t), and z(t)

Definition 4 Y(t) is a column vector that satisfies equation (2.22) which belongs to $C[0, \theta]$.

Theorem 2 The system of equations given by equation (2.22) has a unique solution Y(t) that belongs to $C[0, \theta]$

Proof of Lemma 1. The system of fractional order differential equations (2.16)-(2.18) can be written as follows:

$$I^{1-a}\frac{d}{dt}Y(t) = R_1Y(t) + x(t)R_2Y(t) \tag{2.23}$$

where

$$D_\alpha[Y] = I^{1-a}\frac{d}{dt}Y(t) \tag{2.24}$$

$R_1Y(t)$ indicates that Y(t) evolves with a rate proportional to itself (logistic/ exponential growth/decay)

$x(t)R_2Y(t)$ introduces the interaction between y(t) and x(t) indicating that x(t) influences rate of change Y(t).

Apply the Riemann Louiville Integral to operate I^a to both sides of the equation

$$I^a[D_\alpha[Y]] = I^a(R_1Y(t) + x(t)R_2Y(t) \tag{2.25}$$

Here we solve the fractional integral for Y

$$I = \int_o^\tau Y(\tau)d\tau \ = Y(t) - Y(0) \tag{2.26}$$

Substitute Y(t) -Y(0) for I for the integral

$$Y(t) - Y(0) = I^a(R_1Y(t) + x(t)R_2Y(t)) \tag{2.27}$$

Isolate Y(t) to get the initial conditions

$$Y(t) = Y(0) + I^a(R_1Y(t) + x(t)R_2Y(t)) \tag{2.28}$$

Define operator G[Y(t)] which also belongs on the continuous function C[0,θ]

$$G[Y(t)] = Y(0) + I^a(R_1Y(t) + x(t)R_2Y(t)) \tag{2.29}$$

The solution of Y(t) is a fixed point on the operator G, this satisfies certain properties like:

- Mapping into the space: C[0,θ] so that it operates within the continuous function and since Y(0) and $I^\alpha(R_1Y(t) + x(t)R_2Y(t))$ are continuous, the fractional integral I^α preserves continuity
- Contraction mapping: The operator G is a contraction under certain conditions meaning $||G[Y_1(t)] - G[Y_2(t)]|| \leq L||Y_1(t) - Y_2(t)||$, with $L < 1$, which guarantees a unique solution

where I^a represents the Riemann–Liouville fractional integral.

Consider two solutions $Y(t)$ and $Z(t)$ to analyze the difference between two trajectories:

$$G[Y(t)] - G[Z(t)] = I^a[R_1(Y(t) - Z(t)) + R_2(Y(t) - Z(t))] \tag{2.30}$$

Here we introduce the exponential decay factor and multiply both sides of the equation by e^{-nt}:

$$e^{-nt}[G(Y(t)) - G(Z(t))] = e^{-nt}I^a[R_1(Y(t) - Z(t)) + R_2(Y(t) - Z(t))] \tag{2.31}$$

Expand the fractional integral using the definition of the Riemann–Liouville fractional integral to replace I^a:

(2.32)

$$I^a\left[R_1(Y(t) - Z(t)) + R_2(Y(t) - Z(t))\right] = \frac{1}{\Gamma(\alpha)}\int_0^t (t-c)^{\alpha-1}\left[R_1(Y(c) - Z(c)) + R_2(Y(c) - Z(c))\right]\, dc$$

This formulation ensures that past values $f(c)$ contribute to the present state $f(t)$, weighted by $(t-c)^{\alpha-1}$, which scales historical influence.

Next, apply exponential decay within the integral multiplying by $e^{-n(t-c)}$:

$$\frac{1}{\Gamma(\alpha)}\int_0^t (t-c)^{\alpha-1}e^{-n(t-c)}[Y(c)-Z(c)]e^{-nc}[R_1+uR_2]\,dc \tag{2.33}$$

Now introduce norm bound, it ensures that differences between solutions remain controlled over time

$$\|G[Y(t)]-G[Z(t)]\| \leq \frac{1}{\Gamma(\alpha)}\int_0^t (t-c)^{\alpha-1}e^{-n(t-c)}\|Y(t)-Z(t)\|[R_1+uR_2]\,dc \tag{2.34}$$

Since norm properties allow a unique solution that depend on continuous initial conditions:

$$\|Y(c)-Z(c)\| \leq \|Y(t)-Z(t)\|, \tag{2.35}$$

when applying inequality (2.35) to inequality (2.34), we then factor $\|Y(t)-Z(t)\|$ out of the integral

$$\|G[Y(t)]-G[Z(t)]\| \leq (R_1+uR_2)\|Y(t)-Z(t)\|\frac{1}{\Gamma(\alpha)}\int_0^t (t-c)^{\alpha-1}e^{-n(t-c)}\,dc \tag{2.36}$$

Now the integral evaluates to $\frac{\Gamma(\alpha)}{n^\alpha}$, we can substitute:

$$\|G[Y(t)]-G[Z(t)]\| \leq (R_1+uR_2)\frac{1}{n^\alpha}\|Y(t)-Z(t)\| \tag{2.37}$$

so we can conclude:

$$\|G[Y(t)]-G[Z(t)]\| \leq (R_1+uR_2)\frac{1}{n^\alpha}\|Y(t)-Z(t)\|\int_0^t \frac{\alpha-1}{\Gamma(\alpha)}\,dc \tag{2.38}$$

This bound ensures stability and controls deviations between trajectories.

Substituting the integral back into our expression because it is the definite integral of a constant independent of c integrating from [0,t]:

$$\|G[Y(t)]-G[Z(t)]\| \leq (R_1+uR_2)\frac{1}{n^\alpha}\|Y(t)-Z(t)\|\frac{\alpha-1}{\Gamma(\alpha)}t \tag{2.39}$$

This introduces a bounded scaling factor, which ensures a contraction effect.

Now we establish the contraction property and are observing the structure of the term:

$$\|G[Y(t)]-G[Z(t)]\| \leq (R_1+uR_2)\frac{t}{n^\alpha\Gamma(\alpha)}\|Y(t)-Z(t)\| \tag{2.40}$$

Since the coefficient $\frac{t}{n^\alpha\Gamma(\alpha)}$ acts as a damping factor, it ensures:

$$\|G[Y(t)]-G[Z(t)]\| < \|Y(t)-Z(t)\| \tag{2.41}$$

The integral term accumulates past influences but remains bounded. The contraction property ensures that the operator G smooths out deviations over time. This proves that G satisfies a stability condition, meaning perturbations diminish rather than grow.

Since the operator $G[Y(t)]$ satisfies a contraction property, we guarantee the existence of a unique fixed solution, meaning:

$$G[Y(t)] = Y(t) \tag{2.42}$$

Thus, $Y(t)$ must satisfy the corresponding integral equation.

2.5. Integration of Y(t) using RLI. Using fractional calculus, the solution is expressed in terms of the initial condition $Y(0)$ and the fractional integral I^{α}:

$$Y(t) = Y(0) + I^{\alpha}(R_1 Y(t) + x(t) R_2 Y(t)) \tag{2.43}$$

where I^{α} represents memory-dependent contributions.
Expanding the solution form using fractional integral properties:

$$Y(t) = Y(0) + \frac{t^{\alpha}}{\Gamma(\alpha+1)}[R_1 Y(0) + x(0) R_2 Y(0)] + I^{\alpha+1}[R_1 Y'(t) + x'(t) R_2 Y(t) + x(t) R_2 Y'(t)] \tag{2.44}$$

- The first term $Y(0)$ captures the initial state
- The second term introduces memory scaling using Gamma function properties
- The third term accumulates past interactions via the fractional integral $I^{\alpha+1}$, ensuring long-term dependencies

Thus, the existence of a fixed point leads directly to the solution formulation
Operating equation (2.44) to the initial fractional order derivatives stated in equations (2.13)–(2.15):

$$x(t) = x(0) + \frac{t^{\alpha}}{\Gamma(\alpha+1)}[p_1 x(0)(1 - q x(0)) - p_2 x(0) z(0)] + I^{\alpha+1}[p_1(1 - 2q x(t)) x'(t) - p_2(z(t) x'(t) + x(t) z'(t))] \tag{2.45}$$

$$y(t) = y(0) + \frac{t^{\alpha}}{\Gamma(\alpha+1)}[x(0) z(0) + r d(t) - y(0) - s y(0) z(0)] + I^{\alpha+1}[x'(t) z(t) + x(t) z'(t) - y'(t) - s y'(t) z(t)] \tag{2.46}$$

$$z(t) = z(0) + \frac{t^{\alpha}}{\Gamma(\alpha+1)}[u(1 - v z(0)) - x(0) z(0) - \delta y(0) z(0)] + I^{\alpha+1}[-v z'(t) - x'(t) z(t) - x(t) z'(t)] \tag{2.47}$$

Each population (N, L, T) now follows fractional-order memory dynamics, meaning past interactions influence current behavior. The Gamma function scaling ensures appropriate historical weighting, while the fractional integral term $I^{\alpha+1}$ allows for persistent effects in tumor-immune interactions. The system accounts for biological delays, making the model more realistic than classical differential equations.

2.6. Stability Analysis. Using the nondimensionalized model, we can solve for critical points and find $N_0 = L_0 = T_0 = 0$ for the trivial solution, and for non-zero values we have

$$N_i^* = \frac{p_1 - p_2 \pm \sqrt{4 k_n p_1 q D(t) + p_1^2 - 2 p_1 p_2 - 2 p_1 T(t) + p_2^2 + 2 p_2 T(t) + T^2(t)} - T(t)}{2 p_1 q} \tag{2.48}$$

$$L_i^* = \frac{r D(t) + N(t) T(t)}{s T(t) + 1} \tag{2.49}$$

$$T_i^* = \frac{-\delta L(t) + u \pm \sqrt{\delta^2 L^2(t) - 2\delta u L(t) + 2\delta L(t) N(t) - 4 k_t u v D(t) + u^2 - 2 u N(t) + N^2(t)} - N(t)}{2uv} \tag{2.50}$$

and the Jacobian of the non-dimensionalized model is

$$J = \begin{bmatrix} -2 p_1 q N(t) + p_1 - p_2 - T(t) & 0 & -N(t) & k_n \\ T(t) & -s T(t) - 1 & -s L(t) + N(t) & r \\ -T(t) & -\delta T(t) & -\delta L(t) - 2uv T(t) + u - N(t) & -k_t \\ 0 & 0 & 0 & 0 \end{bmatrix}$$

for the trivial case, the Jacobian becomes

$$J = \begin{bmatrix} p_1 - p_2 & 0 & 0 & k_n \\ 0 & -1 & 0 & r \\ 0 & 0 & u & -k_t \\ 0 & 0 & 0 & 0 \end{bmatrix}$$

This gives us the eigenvalues 0, $p_1 - p_2$, -1, and u. Since u has a positive sign, -1 has a negative sign, and $p_1 - p_2$ could be positive or negative, we can conclude that the trivial case is a saddle point. For the case $L_0 = T_0 = D_0 = 0$, $N_0 = \frac{p_1 - p_2 + \sqrt{p_1^2 - 2p_1p_2 + p_2^2}}{2p_1q} = \frac{1}{q}$

$$J = \begin{bmatrix} -p_1 - p_2 & 0 & -\frac{1}{q} & k_n \\ 0 & -1 & \frac{1}{q} & r \\ 0 & 0 & u - \frac{1}{q} & -k_t \\ 0 & 0 & 0 & 0 \end{bmatrix}$$

This gives us the eigenvalues $-p_1 - p_2$ and -1, which are negative, and $u - \frac{1}{q}$ which could be negative or positive. Since u and q are positive, $u - \frac{1}{q}$ will only be negative when $u < \frac{1}{q}$ or when $q < \frac{1}{u}$. So this set of initial conditions is a saddle point when $q > \frac{1}{u}$ (which corresponds with a NK population cap less than that of the tumor growth rate), and a stable sink when $0 < q < \frac{1}{u}$ (which corresponds with a NK population cap greater than that of the tumor growth rate).

—c—c—c—c— Parameters Range Eigenvalue Stability p_1 $(0, p_2)$ $p_2 - p_1 > 0$ unstable p_1 (p_2, ∞) $p_2 - p_1 < 0$ saddle point p_2 (p_1, ∞) $u + \frac{1}{q}\left(\frac{p_2}{p_1} - 1\right) > 0$ unstable q, p_2 $q \in \left(0, \frac{1}{u}\left(1 - \frac{p_2}{p_1}\right)\right)$, $p_2 \in (0, p_1)$ $u + \frac{1}{q}\left(\frac{p_2}{p_1} - 1\right)$???

For $N = \frac{p_1 - p_2 - T(t)}{p_1 q}$, $L = \frac{N(t)T(t)}{sT(t)+1}$, $T = \frac{u - N(t) - \delta L(t)}{uv}$, $D = 0$,

$$J = \begin{bmatrix} -p_1 + p_2 + \frac{z}{uv} & 0 & -\frac{p_1 - p_2 - \frac{z}{uv}}{p_1 q} & k_n \\ \frac{z}{uv} & -\frac{sz}{uv} - 1 & -\frac{sz\left(p_1 - p_2 - \frac{z}{uv}\right)}{p_1 quv\left(\frac{sz}{uv}+1\right)} + \frac{p_1 - p_2 - \frac{z}{uv}}{p_1 q} & r \\ -\frac{z}{uv} & -\frac{\delta z}{uv} & 2\delta L(t) - \frac{\delta z\left(p_1 - p_2 - \frac{z}{uv}\right)}{p_1 quv\left(\frac{sz}{uv}+1\right)} - u + 2N(t) - \frac{p_1 - p_2 - \frac{z}{uv}}{p_1 q} & -k_t \\ 0 & 0 & 0 & 0 \end{bmatrix}$$

where $z = u - \delta L(t)$

3. Results. Our simulations produced a series of graphs that illustrated important aspects of immune cell dynamics and neuroblastoma tumor progression under various treatment conditions. These visualizations revealed critical trends, including the temporal changes in tumor growth and immune cell populations, and demonstrate the relative efficacy of Cyclophosphamide and IL-2 compared to the control groups. Notably, the combined therapeutic strategy approach consistently outperformed single-agent applications, highlighting the potential benefit of multi-drug treatment approaches.

3.1. Numerical simulation. Numerical simulations were performed in Python using the `NumPy` and `SciPy` libraries. Parameter values were adapted from existing literature (Table 3), while initial immune and tumor cell counts were determined based on relative proportions characteristic of each neuroblastoma risk group (Table 2). Simulations were run across the three patient-risk categories to assess immune response dynamics and treatment effectiveness under varying clinical conditions.

3.1.1. Low-risk neuroblasotma. Low-risk simulations began with relatively small tumor populations and a partially functional immune system. The model evaluated ..

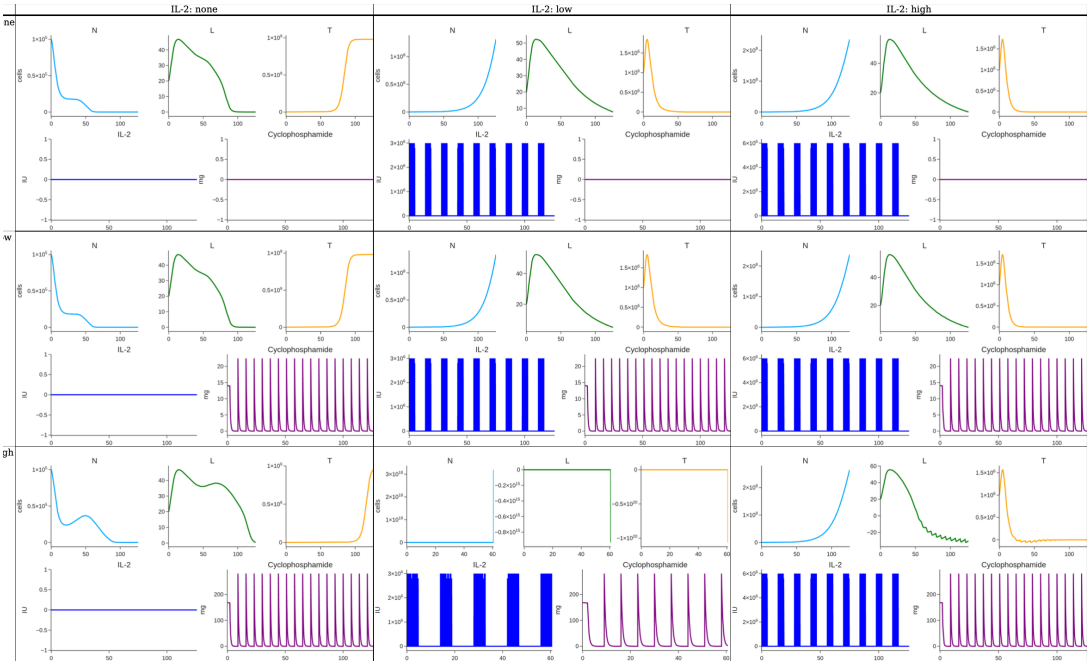

Fig. 1: Low-risk tumor progression under control, IL-2, Cyclophosphamide, and combination treatment.

3.1.2. Intermediate-risk neuroblastoma. Intermediate-risk simulations were initialized with a higher tumor burden and a moderately suppressed immune response ..

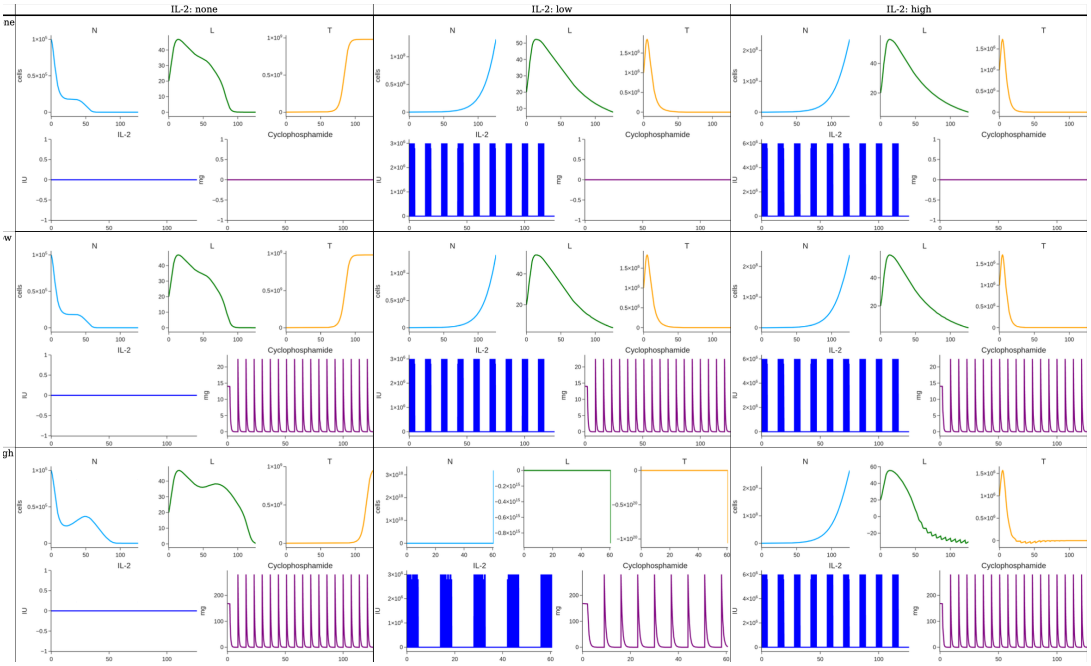

Fig. 2: Intermediate-risk tumor progression under control, IL-2, Cyclophosphamide, and combination treatment.

The simulations for the intermediate-risk group illustrated how ..

3.1.3. High-risk neuroblastoma. High-risk simulations were characterized by aggressive tumor growth and severely compromised immune cell populations.

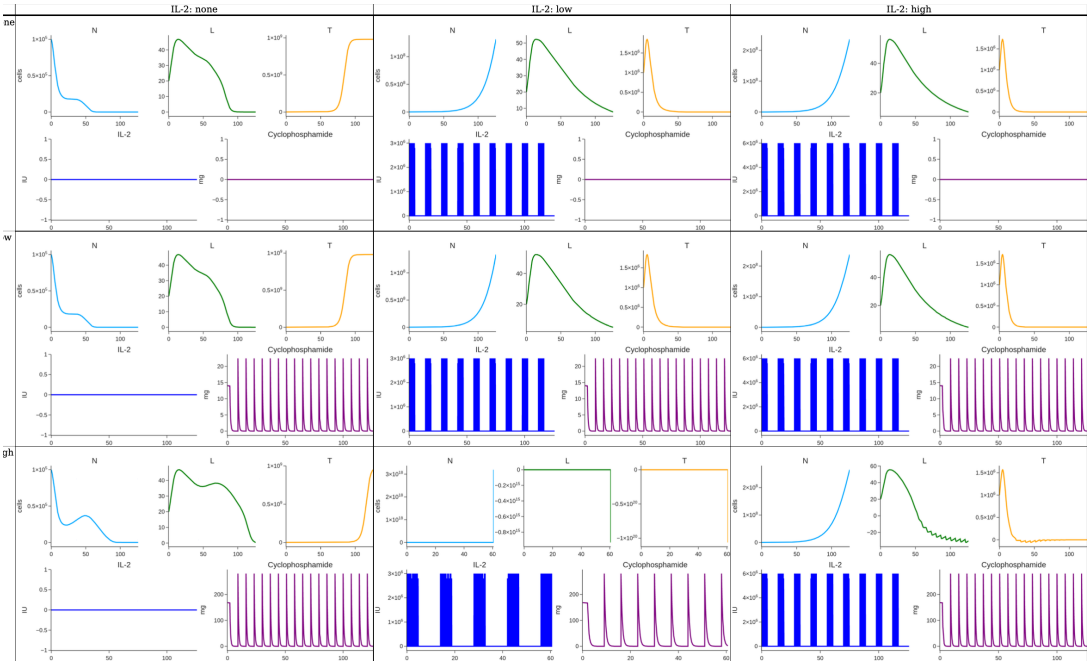

Fig. 3: High-risk tumor progression under control, IL-2, Cyclophosphamide, and combination treatment.

Findings from the high-risk simulations revealed ..

4. Discussion. This study sought to examine the interactions between tumor cells, immune responses, and therapeutic agents in neuroblastoma using a mathematical framework. Our results emphasized and showed the crucial role NK cells and CTLs have in suppressing tumor growth and that both Interleukin-2 (IL-2) and Cyclophosphamide significantly enhance immune-mediated tumor elimination. IL-2 based tumor growth by promoting NK cell proliferation and cytotoxic activity, while Cyclophosphamide exerted both direct tumor-killing effects and immune-stimulating properties. Simulations revealed that each treatment reduced tumor burden through distinct, complementary mechanisms.

By integrating an immunotherapeutic and chemotherapeutic effects, our model highlighted the potential of combined drug therapies. This framework provides valuable insights for treatment optimization and highlights the role mathematical models have in guiding cancer therapies design and clinical decision making.

Data availability. Code and data used in this study is available on GitHub at: https://github.com/JGarza189/neuroblastoma-2025.

Acknowledgements. Our team extends sincere gratitude to Dr. BV Shankara Narayana Rao for her guidance and support throughout the project. Additionally, we would like to thank the Texas A&M High Performance Research Computing Group for portions of this research which were conducted with the advanced computing resources provided by Texas A&M High Performance Research Computing (HPRC).

REFERENCES

[1] Anderson, J., Majzner, R. G., Sondel, P. M. (2022). Immunotherapy of neuroblastoma: Facts and hopes. Clinical Cancer Research, 28(15), 3196–3206.

[2] Arceci, R. J. (2009). The International Neuroblastoma Risk Group (INRG) classification system: An INRG task force report. Yearbook of Oncology, 2009, 162–163.

[3] Bellomo, N., Preziosi, L., Forni, G. (1997). Tumor immune system interactions: The kinetic cellular theory. A Survey of Models for Tumor-Immune System Dynamics, 135–186.

[4] de Pillis, L. G., Gu, W., Radunskaya, A. E. (2006). Mixed immunotherapy and chemotherapy of tumors: Modeling, applications and biological interpretations. Journal of Theoretical Biology, 238(4), 841–862.

[5] de Pillis, L., Fister, K. R., Gu, W., Collins, C., Daub, M., Gross, D., Moore, J., Preskill, B. (2008). Mathematical model creation for cancer chemo-immunotherapy. Computational and Mathematical Methods in Medicine, 10(3), 165–184.

[6] Emadi, A., Jones, R. J., Brodsky, R. A. (2009b). Cyclophosphamide and cancer: Golden Anniversary. Nature Reviews Clinical Oncology, 6(11), 638–647.

[7] Kuznetsov, V. A., Makalkin, I. A., Taylor, M. A., Perelson, A. S. (1994). Nonlinear Dynamics of immunogenic tumors: Parameter estimation and global bifurcation analysis. Bulletin of Mathematical Biology, 56(2), 295–321.

[8] Loose, D., Van de Wiele, C. (2009). The immune system and cancer. Cancer Biotherapy and Radiopharmaceuticals, 24(3), 369–376.

[9] Mueller, S., Matthay, K. K. (2009). Neuroblastoma: Biology and staging. Current Oncology Reports, 11(6), 431–438.

[10] Padder, A., Almutairi, L., Qureshi, S., Soomro, A., Afroz, A., Hincal, E., Tassaddiq, A. (2023). Dynamical analysis of generalized tumor model with Caputo fractional-order derivative. Fractal and Fractional, 7(3), 258.

[11] Postawa, K., Szczygieł, J., Kułażyński, M. (2020). A comprehensive comparison of ODE solvers for Biochemical Problems. Renewable Energy, 156, 624–633.

[12] Pressey, J. G., Adams, J., Harkins, L., Kelly, D., You, Z., Lamb, L. S. (2016). In vivo expansion and activation of T cells as immunotherapy for refractory neuroblastoma. Medicine, 95(39).

[13] Quaranta, V., Weaver, A. M., Cummings, P. T., Anderson, A. R. A. (2005). Mathematical modeling of cancer: The future of prognosis and treatment. Clinica Chimica Acta, 357(2), 173–179.

[14] Rossi, A., Pericle, F., Rashleigh, S., Janiec, J., Djeu, J. (1994a). Lysis of neuroblastoma cell lines by human natural killer cells activated by interleukin-2 and interleukin-12. Blood, 83(5),

[15] Roy, N. K., Bordoloi, D., Monisha, J., Anip, A., Padmavathi, G., Kunnumakkara, A. B. (2017). Cancer — an overview and molecular alterations in cancer. Fusion Genes and Cancer, 1–15.

[16] Smith, V., Foster, J. (2018). High-risk neuroblastoma treatment review. Children, 5(9), 114.

[17] Song, G., Liang, G., Tian, T., Zhang, X. (2022). Mathematical modeling and analysis of Tumor Chemotherapy. Symmetry, 14(4), 704.